

Highly Efficient Iodine Capture by Layered Double Hydroxides Intercalated with Polysulfides

Shulan Ma,^{†,‡} Saiful M. Islam,[‡] Yurina Shim,[‡] Qingyang Gu,[†] Pengli Wang,[‡] Hao Li,[§] Genban Sun,[†] Xiaojing Yang,[†] and Mercouri G. Kanatzidis^{*,‡,§}

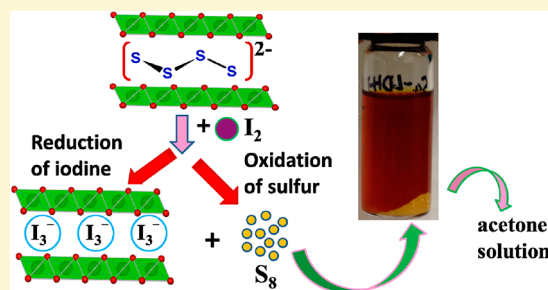
[†]Beijing Key Laboratory of Energy Conversion and Storage Materials, College of Chemistry, Beijing Normal University, Beijing 100875, China

[‡]Department of Chemistry, Northwestern University, 2145 Sheridan Road, Evanston, Illinois 60208, United States

[§]Material Science Division, Argonne National Laboratory, 9700 S Cass Ave, Argonne, Illinois 60439, United States

Supporting Information

ABSTRACT: We demonstrate strong iodine (I_2) vapor adsorption using Mg/Al layered double hydroxide (MgAl-LDH) nanocomposites intercalated with polysulfide (S_x^{2-}) groups (S_x -LDH, $x = 2, 4, 6$). The as-prepared LDH/polysulfide hybrid materials display highly efficient iodine capture resulting from the reducing property of the intercalated polysulfides. During adsorption, the I_2 molecules are reduced to I_3^- anions by the intercalated $[S_x]^{2-}$ groups that simultaneously are oxidized to form S_8 . In addition to the chemical adsorption, additional molecular I_2 is physically captured by the LDH composites. As a result of these parallel processes, and despite their very low BET surface areas, the iodine capture capacities of S_2 -LDH, S_4 -LDH, and S_6 -LDH are ~ 1.32 , 1.52 , and 1.43 g/g, respectively, with a maximum adsorption of 152% (wt %). Thermogravimetric and differential thermal analysis (TG-DTA), energy dispersive X-ray spectroscopy (EDS), and temperature-variable powder X-ray diffraction (XRD) measurements show the resulting I_3^- ions that intercalated into the LDH gallery have high thermal stability (≥ 350 °C). The excellent iodine adsorption performance combined with the facile preparation points to the S_x -LDH systems as potential superior materials for adsorption of radioactive iodine, a waste product of the nuclear power industry.



INTRODUCTION

Nuclear power can be a clean, reliable energy source to meet global population demands if the challenge of nuclear waste pollution can be tackled.^{1,2} Consequently, appropriate management of nuclear waste is a main safety concern associated with the production of nuclear energy. The radionuclide ^{129}I is one of the byproducts and is a hazardous species with its long half-life ($\sim 10^7$ years) that must be captured and reliably stored as nuclear waste. Although ^{131}I is a short-lived (half-life of 8.02 days) radionuclide, it also requires immediate trapping because of its high volatility and involvement in human metabolic processes.^{3–5} Due to the harmful effects of radioactive iodine on human health,^{6,7} their safe and long-term capture using appropriate adsorbents and subsequent storage^{7,8} is extremely important.

There are many existing adsorbent materials for iodine capture, including zerovalent iron,⁹ Illite minerals,¹⁰ Al–O–F materials,¹¹ zeolite-based materials,¹² and functionalized clays.¹³ Ag-based porous zeolitic (AgZ) materials¹² have shown high iodine loading capacity and removal efficiency. In the United States, the most prevalent iodine sorbent studied is AgZ, while Japanese and European researchers have studied $AgNO_3$ -impregnated alumina and silica. However, both AgZ and $AgNO_3$ -impregnated sorbents require silver to bind $I_2(g)$,

which from the cost perspective can be a significant drawback for their extensive use. Porous metal–organic frameworks (MOFs) are another kind of adsorbent for iodine capture,^{14–21} but their relatively low thermal stability²² or steric hindrance of the organic ligands^{23,24} limits their application. Aerogels are a new family for iodine capture.^{25–27} We have developed nonoxide aerogels made with metal sulfides for iodine immobilization and found that these materials are promising as a potential replacement for AgZ.^{28,29} However, the complex preparation processes of aerogels can restrict their widespread use.^{30–32} Thus, it is necessary to develop improved alternative iodine sorbents with higher loading capacity, lower cost, and easier preparation steps than existing materials.

Layered double hydroxides (LDHs) are well studied anion-exchanging materials with low cost and excellent adsorptive properties.³³ They have versatile applications in catalysts,^{34–36} two-dimensional nanoreactors,³⁷ adsorbents for certain guests,³⁸ and other functional materials.^{36,39–41} Considerable efforts have been devoted to the adsorption of environmental contaminants using LDH materials.^{42–44} Functionalized LDHs

Received: October 9, 2014

Revised: November 20, 2014

with anionic cyclodextrin cavities were reported to adsorb molecular iodine.⁴⁵ Recently, we demonstrated the intercalation of polysulfide anions into the LDH gallery to give rise to materials (S_x -LDH) that exhibit outstanding heavy metal ion removal⁴⁶ as well as Hg(0) vapor capture⁴⁷ properties. Here, we show for the first time that the S_x -LDH materials are excellent in achieving rapid iodine capture as well via reduction of the polysulfides.

EXPERIMENTAL SECTION

Materials. MgAl- CO_3 -LDH was prepared by a hexamethylene-tetramine hydrolysis method,^{48,49} and through a NO_3^-/CO_3^{2-} anion-exchange of MgAl- CO_3 -LDH, the MgAl- NO_3 -LDH was obtained.^{48,50} Potassium polysulfides of K_2S_x ($x = 2, 4, 6$) were synthesized by the reactions of K and S in liquid ammonia as reported.³² The S_x -LDH composites were prepared via an exchange of NO_3^- with $[S_x]^{2-}$ as we previously reported.⁴⁶ Using the S_4 -LDH and $Co(NO_3)_2 \cdot 6H_2O$ as reacting materials, LDH- NO_3 - CoS_4 was obtained.⁴⁷

I_2 Vapor Capture. Naturally occurring, nonradioactive I_2 was used in all experiments. Loading was conducted under conditions relevant to fuel reprocessing (350 K/77 °C and ambient pressure). The S_x -LDH composites were tested for I_2 vapor capture in a closed vial setup similar to that previously reported for Hg⁰ adsorption.³² Other materials such as S_8 , K_2S_4 , LDH- NO_3 - CoS_4 , and MgAl- NO_3 -LDH were used for control experiments. An amount of 0.20 g of I_2 was placed on the bottom of a glass vial, and 0.05 g of solid sorbent sample was placed above, supported by conical shaped filter paper at the top of the vial. The vial was capped, wrapped with Teflon tape, and transferred inside a bigger glass vial in order to prevent leakage of I_2 vapor and to ensure homogeneous transfer of heat to the inner vials. The bigger vial containing several smaller vials was placed in the sand bath at a temperature of ~ 75 °C. After a period of time (1–2 days), the sand bath was cooled to room temperature, and the sample mass difference (before and after adsorption) was measured to estimate the captured amount of iodine. Elemental distribution maps using energy dispersive X-ray spectroscopy (EDS) and X-ray photoelectron spectroscopy (XPS) analyses were done to confirm the iodine presence in the samples after adsorption.

Physical Characterization and Chemical Analyses. Powder X-ray diffraction (XRD) patterns were collected with a Phillips X'pert Pro MPD diffractometer using Cu $K\alpha$ radiation, at room temperature, with a step size of 0.0167° , a scan time of 15 s per step, and 2θ ranging from 4.5 to 70° . The generator setting was 40 kV and 40 mA. Variable temperature XRD patterns were collected using a step size of 0.0167° , a scan step time of 20 s, and a 2θ range of 4.5 to 70° . The temperature ascending rate of 20 °C/min was used, and the holding time at each selected temperature was 3 min. The temperature was raised in 50 °C steps from 50 to 600 °C. The change of temperature was controlled by the TCU2000 Temperature Control Unit (Anton Parr Co.). Fourier transformed infrared (FT-IR) spectra of the samples were recorded on a Nicolet-380 Fourier-Transform infrared spectrometer using the KBr pellet method. Raman spectra were taken on a microscopic confocal Raman spectrometer, using a 633 nm He-Ne laser. Thermogravimetric and differential thermal analysis (TG-DTA) measurements were performed with a ZRY-2P thermal analyzer in an air atmosphere. Scanning electron microscopy (SEM), elemental distribution mapping, and energy dispersive spectroscopy (EDS) measurements were carried out using a Hitachi S-4800 microscope. UV-vis absorption spectra were recorded on a TU-1901 spectrophotometer using suspensions of I-loaded samples in acetonitrile.

The surface area was measured by nitrogen adsorption/desorption at 77 K at relative pressures (P/P_0) in the range of 0.05 – 0.30 with a Micromeritics Tristar II system, using the Brunauer-Emmett-Teller (BET) model. The samples were degassed at 298 K under a vacuum for 12 h before analysis to remove any adsorbed impurities. XPS studies were performed using a Thermo Scientific ESCALAB 250 Xi spectrometer equipped with a monochromatic Al $K\alpha$ X-ray source (1486.6 eV) and operated at 300 W. Samples were analyzed under a

vacuum ($P < 10^{-8}$ mbar), whereas survey scans and high-resolution scans were collected using a pass energy of 25 eV. Binding energies were referred to the C 1s binding energy at 284.6 eV. A low-energy electron flood gun was employed for charge neutralization. Prior to XPS measurements, powders were pressed on copper foil and mounted on stubs and successively put into the entry-load chamber to pump. Fitting of the peaks was made by using the Avantage software.

The metal contents of the solid samples were determined using inductively coupled plasma atomic emission spectroscopy (ICP-AES, Jarrel-ASH, ICAP-9000). Solutions of 0.1 M HNO_3 were used to dissolve the solids. CHN analyses of the samples were conducted using an Elementar Vario EL elemental analyzer.

RESULTS AND DISCUSSION

Characterization of S_x -LDH and LDH- NO_3 - CoS_4 . The synthesis of polysulfide/LDH materials was accomplished via

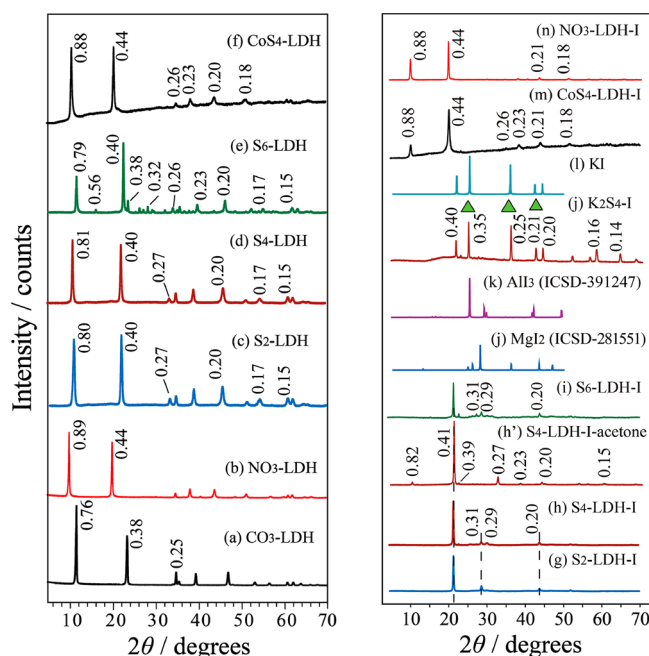
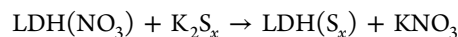


Figure 1. XRD patterns of the precursors (a) CO_3 -LDH and (b) NO_3 -LDH; the exchanged products (c) S_2 -LDH, (d) S_4 -LDH, (e) S_6 -LDH, and (f) LDH- NO_3 - CoS_4 , I-adsorbed samples of (g) S_2 -LDH-I, (h) S_4 -LDH-I, (i) S_6 -LDH-I, (j) K_2S_4 -I, (k) KI, (l) LDH- CoS_4 -I, and (m) NO_3 -LDH-I. The d values are given in nanometers.

an ion-exchange reaction of NO_3^- with $[S_x]^{2-}$ according to the scheme:⁴⁶



Based on ICP, CHN analyses, and charge balance considerations, the compositions of S_2 -LDH, S_4 -LDH, and S_6 -LDH were estimated to be $Mg_{0.67}Al_{0.33}(OH)_2(S_2)_{0.14}(NO_3)_{0.01}(CO_3)_{0.02} \cdot 0.8H_2O$, $Mg_{0.67}Al_{0.33}(OH)_2(S_4)_{0.13}(NO_3)_{0.01}(CO_3)_{0.03} \cdot 0.8H_2O$, and $Mg_{0.67}Al_{0.33}(OH)_2(S_6)_{0.11}(NO_3)_{0.01}(CO_3)_{0.05} \cdot 0.3H_2O$, respectively. The CO_3^{2-} anions in the formula are adventitious and are introduced from air or water because of the high affinity of CO_2^{2-} for LDH layers.⁴⁸ After ion-exchange of $[S_x]^{2-}$ with NO_3^- , the basal spacing (d_{basal}) of 0.89 nm in NO_3 -LDHs increased to 0.80/0.81/0.79 nm (Figure 1c–e). In view of the thickness of the LDH layer (0.48 nm) and d_{basal} values of S_x -LDHs (~ 0.80 nm), the observed gallery height of ~ 0.32 nm (=

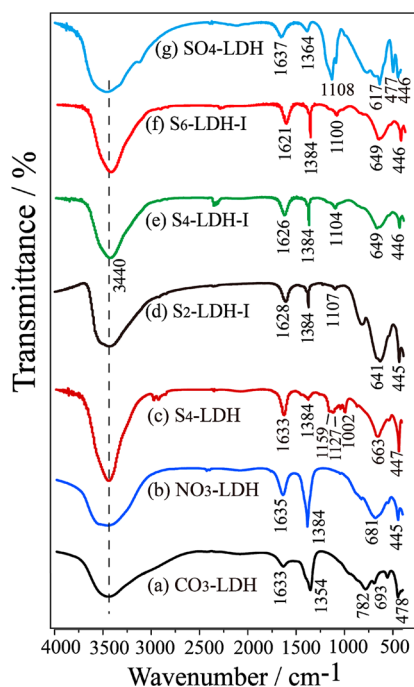


Figure 2. FT-IR spectra of (a) CO_3 -LDH, (b) NO_3 -LDH, (c) S_4 -LDH, I-laden samples of (d) S_2 -LDH-I, (e) S_4 -LDH-I, (f) S_6 -LDH-I, and (g) SO_4 -LDH.

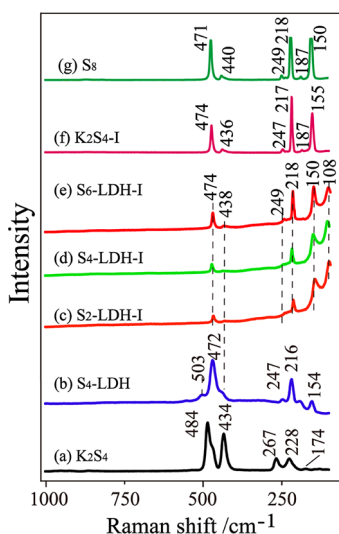


Figure 3. Raman spectra of (a) K_2S_4 , (b) S_4 -LDH, (c) S_2 -LDH-I, (d) S_4 -LDH-I, (e) S_6 -LDH-I, (f) K_2S_4 -I, and (g) S_8 .

0.80–0.48) suggests a similar flat lying arrangement of zigzag $[\text{S}_x]^{2-}$ anions in the interlayer.⁴⁷ For S_6 -LDH, a clear Bragg peak at 0.38 nm is possibly associated with the (006) reflection of CO_3 -LDH. Changing the starting $\text{K}_2\text{S}_6/\text{LDH}$ ratios did not remove the 0.38 nm peak. Thus, steric hindrance from the $[\text{S}_6]^{2-}$ chains may prevent the coexistence of CO_3^{2-} with $[\text{S}_6]^{2-}$ in the gallery, ultimately forcing CO_3^{2-} to form a separate phase (CO_3 -LDH), whose (003) reflection at 0.76 nm may overlap with the 0.79 nm peak (the (003) reflection of S_6 -LDH phase). It is noteworthy that in S_2 -LDH and S_4 -LDH the intensity of (003) and (006) reflections is similar, which is due to the presence of the high electron density S_x^{2-} species in the gallery. In S_6 -LDH, the 006 reflection is stronger than the (003) reflection, because of the even higher electron density of the

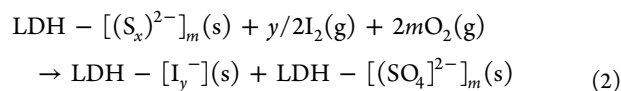
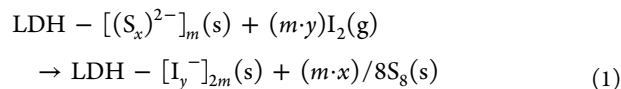
longer S_6^{2-} ions in the gallery. For $\text{LDH}-\text{NO}_3-\text{CoS}_4$ (Figure 1f), the 0.88 nm d_{basal} is close to that of NO_3 -LDH and suggests that the NO_3^- resides in the gallery while the “ CoS_4 ” exists as an amorphous phase.⁴⁷

The IR spectra (Figure 2) provide clear evidence for the ion-exchange reaction. The absorption bands at 1354 cm^{-1} (Figure 2a) and 1384 cm^{-1} (Figure 2b) respectively correspond to CO_3^{2-} and NO_3^- . In the S_x -LDH samples, the 1384 cm^{-1} band (Figure 2c) is very weak, implying a nearly complete substitution of NO_3^- by $[\text{S}_x]^{2-}$. The double charged $[\text{S}_x]^{2-}$ provides a stronger driving force for the ion-exchange than the singly charged NO_3^- .^{48,52–54} Moreover, the bands at 663 and 447 cm^{-1} (Figure 2c) assigned to $\nu(\text{M}-\text{O})$ and $\delta(\text{O}-\text{M}-\text{O})$ vibrations arise from the LDH layer in S_4 -LDH.⁴⁶ Raman spectra (Figure 3) further demonstrate the presence of $[\text{S}_x]^{2-}$ anions as a result of the successful ion exchange. As shown in Figure 3a, the peaks at 228, 267, 434, and 484 cm^{-1} correspond to the symmetric and asymmetric S–S vibrations of K_2S_4 ,⁵⁵ and after intercalation, these main S–S vibration bands (Figure 3b) remain, with only a little shift and some change of the relative intensity.

XPS spectra were employed (Figure 4) to probe the polysulfides in LDH. The assignment of the binding energies for S_x -LDH is summarized in Table 1. Figure 4a,d,g reveal broad bands in the range of 159–166 eV, indicating the presence of multiple oxidation states of sulfur as expected for a polysulfide.^{56,57} In S_6 -LDH, the weak peak at 167.6 eV (peak 4 in Figure 4g) suggests a small degree of oxidation of $[\text{S}_x]^{2-}$ to $\text{SO}_3^{2-}/\text{SO}_4^{2-}$.⁵⁸ The XPS spectra of the materials after I_2 adsorption reveal the occurrence of I based peaks and will be discussed below.

Iodine Capture. The iodine vapor capture by S_x -LDH is rapid as judged from the color change of the solid samples from yellow to brown within a period of 30 min. A control experiment carried out with $\text{MgAl}-\text{NO}_3$ -LDH showed no color change even after 3 days of exposure to iodine vapor, highlighting the key role of the intercalated polysulfides in the iodine adsorption process. The capture capacity for iodine was directly obtained by weighing the samples before and after adsorption. The adsorption capacities for S_2 -LDH, S_4 -LDH, and S_6 -LDH were calculated to be 1.32, 1.55, and 1.43 g/g, respectively (see Table 2). The theoretical chemisorption capacities listed in Table 2 are based on the balanced reaction of S_x -LDH with I_2 , in which the molar ratio of $[\text{I}_y]^-/[\text{S}_x]^{2-}$ is 2 based on their charge ratio of 2.

For reactions between I_2 and S_x -LDH, there are two possible schemes:



According to IR spectra (Figure 2d–f), there are no clear observable $[\text{SO}_4]^{2-}$ bands around 1108 cm^{-1} as in Figure 2g. XRD results also do not show the d_{basal} of 0.87 nm for SO_4 -LDH.^{48,59,60} Since there is no SO_4 -LDH phase observed, eq 2 is ruled out, and therefore S_8 is the most likely oxidation product as shown in eq 1.

Additionally, in eq 1, the polyiodide anions of $[\text{I}_3]^-$ and/or $[\text{I}_5]^-$ can form,⁴⁵ while molecular I_2 is adsorbed on the surface

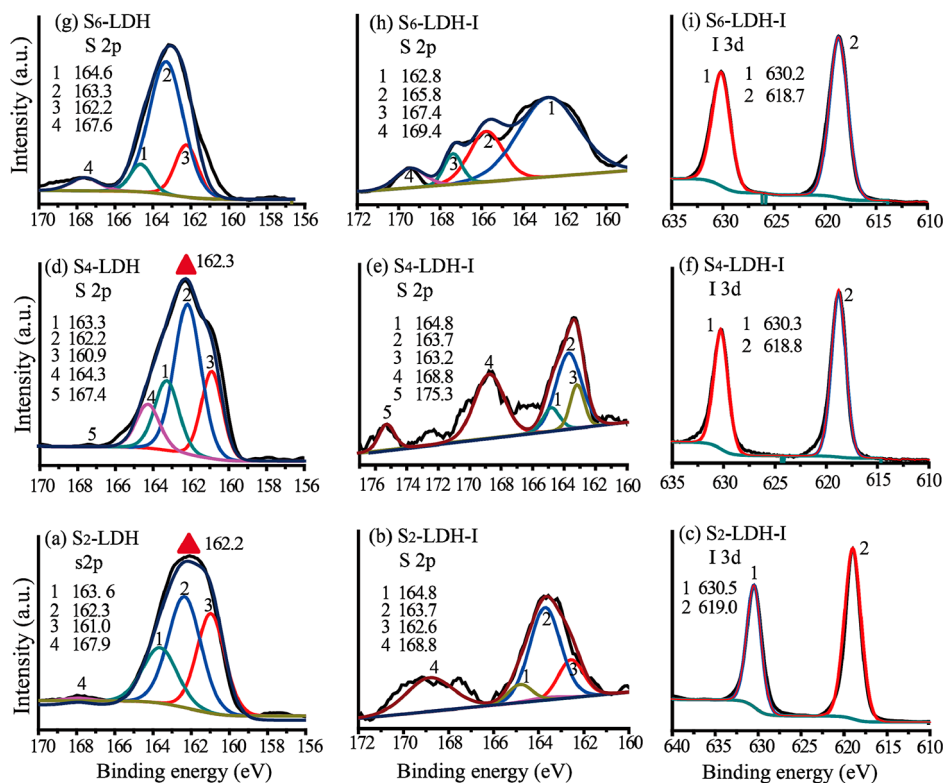


Figure 4. XPS spectra for S 2p and I 3d with deconvolution of corresponding XPS peaks. Parts a, d, and g correspond to those before adsorption (S_x -LDH), and the remaining are those after iodine adsorption (S_x -LDH-I).

Table 1. XPS Data and Assignment of S and I States for S_x -LDH before/after Adsorption

		binding energy (eV) ^a	assignment
S_2 -LDH	before I adsorption	163.6	2p of S^0
		162.3/161.0	2p of $[S_n]^{2-}$
	after I adsorption	164.8/163.7	2p of S^0
		162.6	2p of $[S_n]^{2-}$
		168.8	2p of S^{6+} (SO_4^{2-})
		630.5	$3d_{3/2}$ of I
S_4 -LDH	before I adsorption	163.3	2p of S^0
		162.2	2p of S^{1-}
	after I adsorption	160.9	2p of S^{2-}
		164.8/163.7	2p of S^0
		163.2	2p of $[S_n]^{2-}$
		168.8	2p of S^{6+} (SO_4^{2-})
S_6 -LDH	before I adsorption	163.3	2p of S^0
		162.2	2p of $[S_n]^{2-}$
	after I adsorption	162.8	2p of $[S_n]^{2-}/S^0$
		167.4/169.4	2p of SO_3^{2-}/SO_4^{2-}
		630.2	$3d_{3/2}$ of I_n^-
		618.7	$3d_{5/2}$ of I_n^-

^aThe binding energies were obtained from the deconvoluted peak positions.

of LDH. Raman spectroscopy was employed to detect the $[I_x]^-$ species.⁴⁵ For $[I_3]^-$, an intense band at ~ 110 cm^{-1} (ν_1 , symmetric stretch) is expected,^{45,61,62} and sometimes a 150 cm^{-1} band assigned to Fermi resonance is also present,⁶² but

Table 2. I_2 Vapor Capture Results for S_x -Containing Samples^a

samples	adsorption capacity ^b		theoretical chemisorption capacity ^c	
	g/g	wt %	g/g	wt %
S_2 -LDH	1.32	132%	1.26	126
S_4 -LDH	1.55	155%	1.05	105
S_6 -LDH	1.43	143%	0.93	93
K_2S_4	0.84	84%	1.25 ^d	125
S_8	no			
LDH- NO_3 - CoS_4	no			
NO_3 -LDH	no			

^aThree samples were used to evaluate these results. ^bThe values were obtained from the mass difference of samples by weighing them before and after iodine adsorption. Sample: 0.05 g. I_2 : 0.20 g. T : 60 °C. Time: 24 h. ^cThese values were based on the reacting formula: LDH- $[(S_x)^{2-}]_m + 3m \cdot I_2 \rightarrow LDH[I_3^-]_{2m} + (m \cdot x)/8 \cdot S_8$, where moles of I_3^- are double those of $[S_x]^{2-}$. S_2 -LDH: $1/85 \times 0.14 \times 2 \times 380.7 = 1.26$ g/g. S_4 -LDH: $1/93 \times 0.13 \times 2 \times 380.7 = 1.05$ g/g. S_6 -LDH: $1/90 \times 0.11 \times 2 \times 380.7 = 0.93$ g/g. ^dThe value was deduced by the reaction formula of $2K_2S_4 + 2I_2 \rightarrow 4KI + S_8$.

for $[I_5]^-$, a band at $167/168$ cm^{-1} corresponding to coordinated iodine should appear.^{62,63} Since our present I-laden samples show an intense band at 108 cm^{-1} (~ 110 cm^{-1}) but not at $167/168$ cm^{-1} band (Figures 3c–e), it suggests the presence of $[I_3]^-$ rather than $[I_5]^-$. Nevertheless, based on calculated vibrational frequencies of I_5^- ,⁶² the 150 cm^{-1} band may be due also to some I_5^- . In K_2S_4 -I, there are no bands corresponding to any $[I_x]^-$, because the anion of the product in the reaction ($K_2S_4 + 2I_2 \rightarrow 4KI + S_8$) is the only I^- . Although $[IO_3]^-$ may also be a potential product because of possible air exposure at the beginning of the adsorption tests, its signature⁵⁸

Table 3. Iodine Adsorption Capacity of Various Absorbents in This Work and References^a

	iodine state	T (°C)	surface area (m ² /g)	capacity (wt %)	iodine form	reference
S _x -LDH ^b	I ₂ (g)	70	9–13	132–155	I ₂ /I _n -LDH ^c	this work
Ag@Mon-POF ^d	I ₂ (g)	70	690	25	AgI ^e	27
ZIF-8 ^f	I ₂ (g)	77	1630 ⁷⁴	125	I ₂ ^g	69
SnS ₈ /SnS _p ^h	I ₂ (g)	125	270	67–68	SnI ₄ (S ₈) ₂ ⁱ	28
SnS ₃₃ ^j	I ₂ (g)	125	13	33	SnI ₄	28
SnS ₃₀ ^j	I ₂ (g)	125	23	53	SnI ₄ (S ₈) ₂	28
Cg-5C ^k	I ₂ (g)	140	360	239 (20 days)	I ₂ ^l	25
Cg-5P ^k	I ₂ (g)	140	287	87	I ₂ ^l	25
(BYA) ₂ [PbBr ₄] ^m	I ₂ (g)	-	-	75	BYA-I ₂ ⁿ	75
[(CH ₃) ₂ NH ₂] _{1.66} [Cd _{1.84} Na _{0.66} (BDC) ₃].DMF.0.5EtOH ^o	cyclohexane solution of I ₂	R. T.	-	17	I ₂ ^p	22
MIL-53 ^q	cyclohexane solution of I ₂	R. T.	-	20–60	I ₂ ^r	
[Cu ₄ I ₃ -(DABCO)] ₂ I ^s	cyclohexane solution of I ₂	R. T.	-	118	I ⁻ /I ₂ ^t	64
MgAl-NO ₃ -LDH ^u	I ₂ water solution	R. T.	10	1	I _n ^v	70

^aThe ‘-’ refers to no related data reported in the reference. ^bLDH intercalated with polysulfides. ^cIntercalation and electrostatic interaction of iodine anion and LDH layer. ^dAg@Mon-POF: polymeric organic framework (Mon-POF) adsorbs Ag⁺ to deposit Ag nanoparticles into the pores. ^eReaction of I₂ and Ag to form AgI. ^fZeolitic imidazolate framework-8. ^gInteractions between polarizable I₂ and MeIm (2-methylimidazole) ligand, i.e. I⁻⋯H and I⁻⋯C contacts. ^hSn₂S₃ chalcogen granule (SnS_g) or powder (SnS_p). ⁱIodine binding with S_n. ^jPAN(polyacrylonitrile)-chalcogen hybrid. ^kPt-Ge-S chalcogen aerogels. ^lPearson’s HSAB principle based on the affinity of a soft Lewis base such as chalcogen (i.e., S, Se) for a soft Lewis acid such as I₂(g). ^mHybrid perovskite (BYA)₂[PbBr₄] in which the BYA is an alkyne-ammonium group. ⁿFormation of BYA-I₂ molecules via covalent C–I bonds. ^oEight-connected self-interpenetrating porous MOF. ^pCharge-transfer (CT) between I₂ and π -electron walls. ^qAl-based MOFs ^rCharge transfer complexes between electron donors as amino and iodine. ^sCopper(I) halide-based MOF, DABCO = N,N'-dimethyl-1,4-diazabicyclo[2.2.2]octane. ^tAdsorption and intermolecular interactions. ^uTreatment of wastewater containing high concentrations of iodine ^vElectrostatic attraction of iodine and LDH layers.

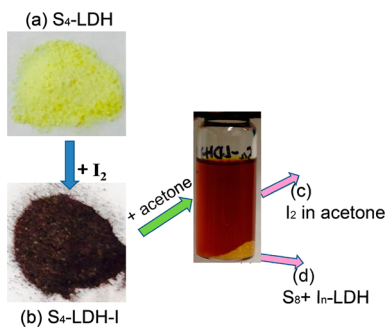


Figure 5. Photographs showing the state of samples before and after iodine adsorption.

is not observed in the XPS data (Figure 4). Based on the above analyses, the product of iodine absorption by S_x-LDH should be I₃⁻.

The UV/vis absorption bands appearing at 295 and 360 nm further verify the presence of [I₃]⁻, which correspond to the spin and symmetry-allowed σ - σ^* and π - σ^* transitions.^{64–67} Thus, the iodine adsorption process of S_x-LDH involves the redox reaction and subsequent intercalation according to eq 1. That is, the I₂ molecules are reduced by polysulfides to produce I₃⁻ anions, which ultimately intercalate into the LDH interlayer; meanwhile, the [S_x]²⁻ are oxidized by I₂ to form S₈. On the basis of the affinity order of anions to the LDH layer (CO₃²⁻ > SO₄²⁻ > OH⁻ > F⁻ > Cl⁻ > Br⁻ > NO₃⁻ > I⁻),⁴⁸ I⁻ or I_n⁻ ions have very low affinity for the LDH layer; therefore, generally, it

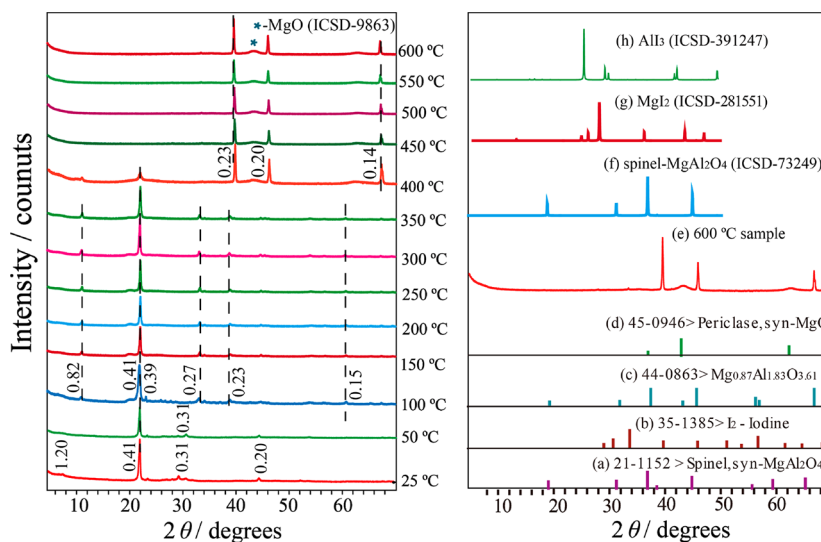


Figure 6. Variable temperature XRD patterns of S₄-LDH-I heated in air and standard calculated patterns of related products.

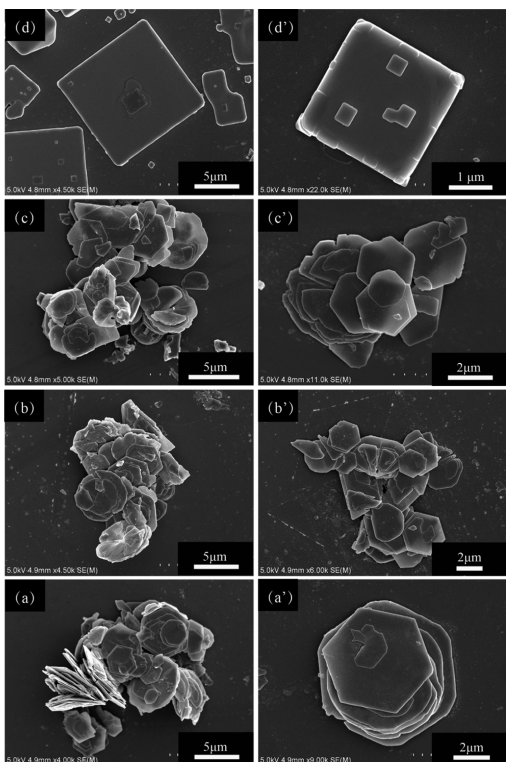
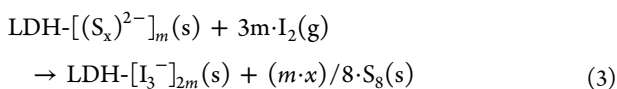


Figure 7. SEM images of I-laden samples of (a,a') S_2 -LDH-I, (b,b') S_4 -LDH-I, (c,c') S_6 -LDH-I, and (d,d') K_2S_4 -I.

is very difficult to synthesize I_n^- intercalated LDH. Bastianini et al.⁶⁸ studied the intercalation of molecular iodine in non-aqueous solutions into LDH-Cl but could not obtain a pure LDH-I hydrotalcite phase, because the LDH had a poor affinity for I^- ions which prevented complete I^-/Cl^- exchange. Sasaki et al.⁶⁷ also reported the intercalation of I_3^- into CoFe-LDH, for which the I_3^- ions are the redox active species used for partial oxidation of Co^{2+} to Co^{3+} . All these cases suggest that it is difficult to obtain I_n^- intercalated LDH through normal anion exchange methods. Therefore, the I_2 adsorption processes we describe here also amount to a facile method for preparing such iodide intercalated LDH materials.

The theoretical chemisorption capacities for iodine are determined based on the amount of $[S_x]^{2-}$ in S_x -LDH and the reaction



in which there are twice as many equivalents of I_3^- as $[S_x]^{2-}$. Taking S_2 -LDH as an example with its molecular weight of 85, the amount of $[S_2]^{2-}$ is 0.14 mol, and the weight of I_3^- is 380.7 g. Therefore, the chemisorption capacity is calculated to be 1.26 g/g ($= 1/85 \times 0.14 \times 2 \times 380.7$). The details with some examples and the results are listed in Table 2. As shown in the table, the amounts of iodine captured by both chemisorption and physisorption are all greater than the calculated theoretical chemisorption amounts. In comparison to the reported MOF materials where the highest I_2 uptake loading is 125% (wt %),⁶⁹ the S_x -LDH materials give higher adsorption capacities of 132–155%. Table 3 compares the I_2 adsorption capacities of some reported adsorbents and S_x -LDH materials in this work. The adsorption capacities of S_x -LDH are much higher than those of

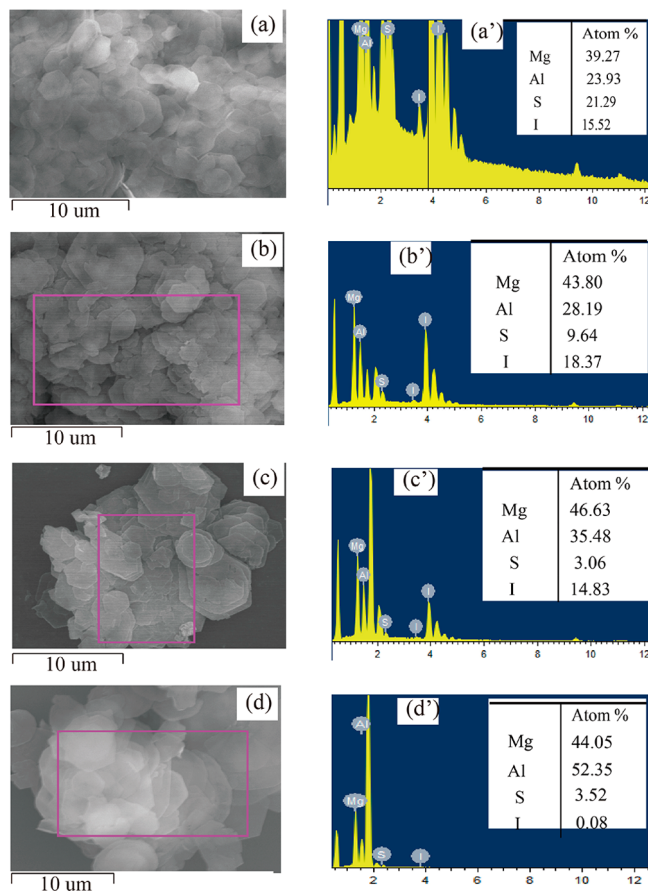


Figure 8. (a) SEM image, (a') EDS and average chemical composition of S_4 -LDH-I, and corresponding SEM image and EDS data for the heated samples in the air for 1 h under temperatures of (b, b') 150 °C, (c, c') 350 °C, (d, d') 450 °C.

$Ag@Mon-POF$,²⁷ the zeolitic imidazolate framework-8 (ZIF-8),¹⁵ and Cg-SP (Pt-Ge-S chalcogen aerogel).²⁵

Nearly all of the previously reported iodine adsorbing materials have very large surface areas (287–1630 m^2/g), and it is this physical surface characteristic that mainly contributes to the final capture result. The very high adsorption capacity of our materials occurs despite the low surface areas of only $\sim 10 m^2/g$ (Figure S2, Supporting Information) and suggests that the chemically functional polysulfides groups play a critical role in iodine adsorption (rather than the physical surface properties alone). Both the reductive property of polysulfides and the intercalative function of LDH materials contribute to the total high iodine capture. For pure $MgAl-NO_3-LDH$ (lacking the polysulfide guests), the adsorption capacity is only $\sim 1\%$.⁷⁰ Detailed information and comparisons between adsorbents and iodine at different states as well as the iodine form after adsorption are summarized in Table 3. This unique property of our materials provides important insights for designing additional superior iodine adsorbents in the future.

To further validate our results with S_x -LDH, several control experiments were carried out using various key materials such as crystalline S_8 , crystalline K_2S_4 , $LDH-NO_3-CoS_4$, and $MgAl-NO_3-LDH$ as adsorbents. These materials lack one or more key properties the S_x -LDH systems have: S_8 has S–S bonding, but its oxidation state is zero; K_2S_4 exhibits S–S bonds similar to those in S_x -LDH and possesses the reductive capacity to capture I_2 , but it lacks the LDH layer; $LDH-NO_3-CoS_4$ has

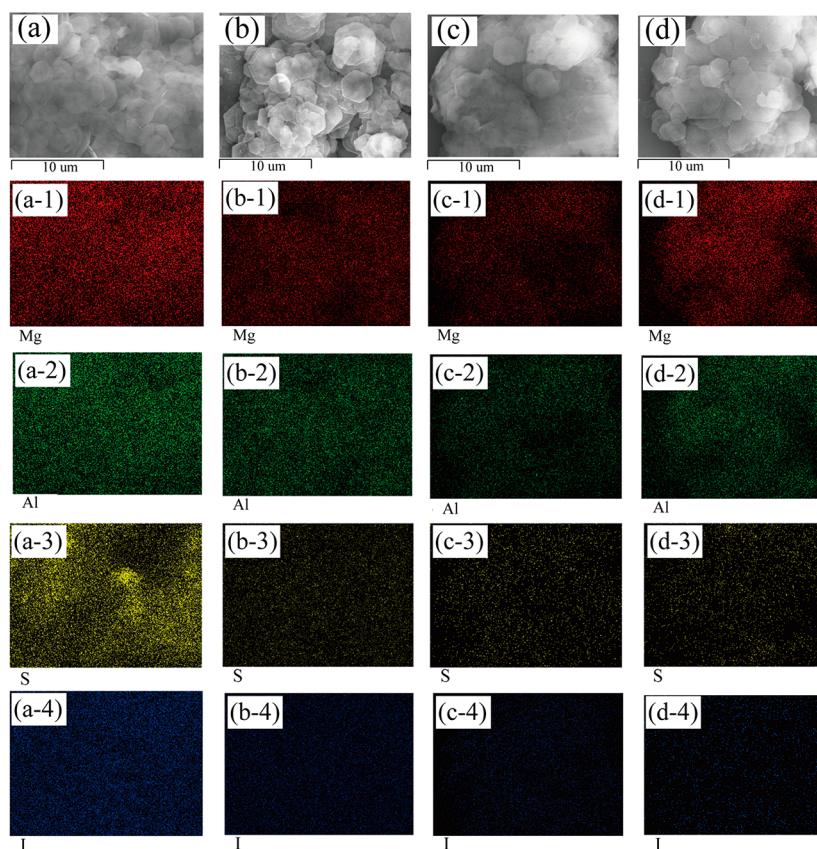


Figure 9. SEM and elemental distribution maps of S_4 -LDH-I and the heated samples in the air for 1 h: (a) SEM of S_4 -LDH-I and a-1–a-4 maps for Mg, Al, S, I. (b) SEM of 150 °C-heated sample, and b-1–b-4 maps for Mg, Al, S, I. (c) SEM of 350 °C-heated sample, and c-1–c-4 maps for Mg, Al, S, I. (d) SEM of 450 °C-heated sample, and d-1–d-4 maps for Mg, Al, S, I.

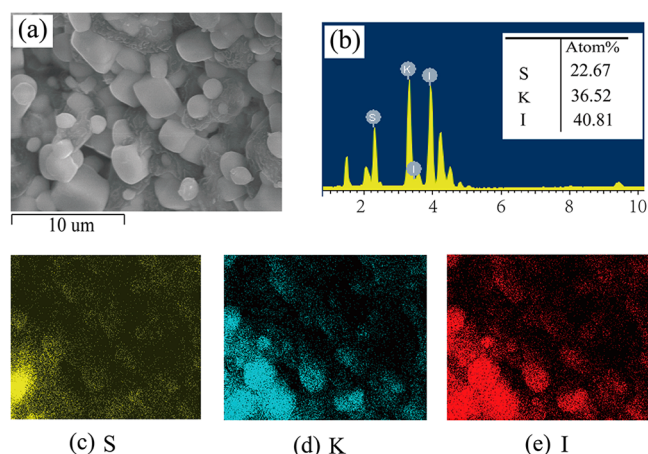


Figure 10. (a) SEM image of K_2S_4 -I. (b) EDS and average chemical composition for the area a. (c–e) Elemental distribution maps for S, K, I in a.

polysulfide groups, but they are coordinated to Co^{2+} and thus have a weak reductive capacity; $MgAl-NO_3$ -LDH is the starting material and has only LDH layers with no reductive capacity. As seen in Table 2, crystalline K_2S_4 does display some iodine capturing capability but it is lower compared to its theoretical chemisorption capacity and much lower than that of S_x -LDH. $LDH-NO_3-CoS_4$ and S_8 show even lower iodine capture. The limited iodine capture by $LDH-NO_3-CoS_4$ is possibly from the coordinated S species that inhibit the reaction with iodine. In the absence of polysulfide species, the parent materials $MgAl-$

NO_3 -LDH shows no iodine adsorption. All of these control experiments emphasize the importance of the intercalated polysulfide sites (in the gallery space of LDH) in achieving the high iodine adsorption efficiency.

Structures and Morphologies of I-Laden Samples. As shown in the XRD patterns of Figure 1g–i, after iodine adsorption, the samples (labeled as S_x -LDH-I) reveal a strong Bragg reflection at 0.41 nm and low intensity reflections at 0.31, 0.20, and 0.17 nm. The 0.41 nm reflection is consistent with the (006) reflection of the iodide intercalated $MgAl$ -LDH with a d_{basal} of 0.82 nm,⁴⁸ while the (003) reflection at 0.82 nm is unobserved. This results from the very heavy nature of the iodine atoms in $[I_3]^-$ ions, which places massive electron density on the (006) plane of the crystal structure. Bastianini et al.⁶⁸ also found that in I_n^- intercalated $ZnAl$ -LDH ($d_{basal} = 0.81$ nm), the relative intensity of the (006) reflection is stronger than other (00*l*) reflections, and this was interpreted as the increase in electron density of the interlayer region, due to the presence of heavy iodine atoms halfway between adjacent brucite sheets.

When organic solvents such as acetone are used to wash the S_4 -LDH-I sample, leaching of I_2 is observed forming a red solution (Figure 5c) along with an insoluble yellow solid (Figure 5d). The solids, separated by filtration, showed XRD patterns with an obvious Bragg peak at 0.82 nm (Figure 1h). The dissolution reaction in acetone could be $LDH-[I_3]^- \xrightarrow{\text{acetone}} LDH-I^- + I_2$, and the remaining solid is $LDH-I^-$. The electron density of the interlayer I^- ions is lower than $[I_3]^-$, and this results in the occurrence of the (003) reflection at 0.82 nm.

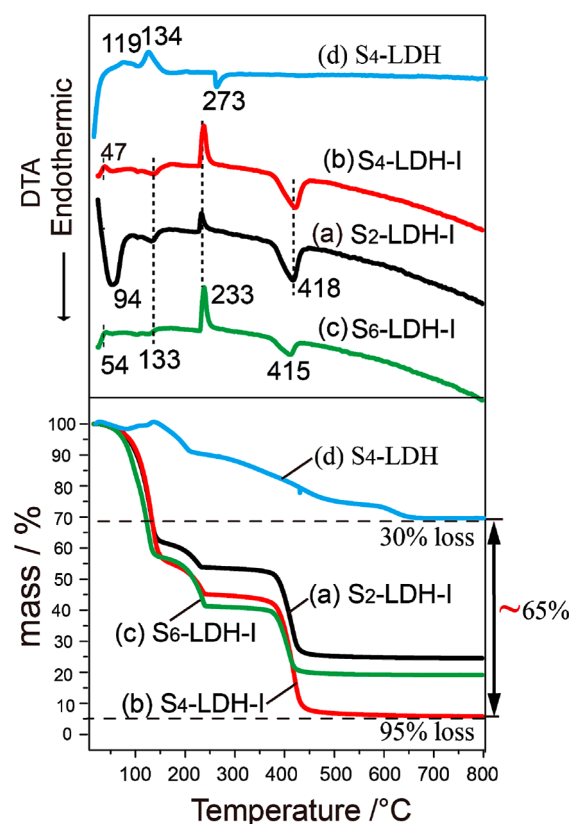


Figure 11. TGA-DTA curves of (a) S_2 -LDH-I, (b) S_4 -LDH-I, (c) S_6 -LDH-I, and (d) S_4 -LDH (in air).

This is consistent with simulated PXRD patterns of model structures of LDH by Kamath et al.⁷¹ The yellow color of the solids comes from S_8 . The variable temperature XRD patterns (Figure 6) of S_4 -LDH-I showed an obvious peak at 0.82 nm when heated up to 400 °C, similar to that observed in the acetone-washed sample (Figure 1h). This further verifies the formation of I^- intercalated LDH, resulting from the decomposition of $[I_3]^-$ and the removal of molecular I_2 by heating or acetone washing.

The Raman spectra show a series of peaks corresponding to the S_8 phase (Figure 3g) verifying the oxidation of $[S_x]^{2-}$ to S_8 . XPS spectra (Figure 4) also showed the formation of S_8 and the presence of iodine after adsorption. There were very strong and clear I 3d peaks (~ 630 eV for I $3d_{3/2}$ and ~ 619 eV for I $3d_{5/2}$), which are consistent with the 3d binding energies of iodine ions.⁵⁸ Similar to the starting materials, the I-laden samples showed S 2p peaks corresponding to various oxidation states of S. The strongest peak appeared at 163.7 [peak 2] in S_2 -LDH-I, 163.7 [peak 2] in S_4 -LDH-I, and 162.8 [peak 1] in S_6 -LDH-I corresponding to the binding energies of S 2p for S_n^{o58} confirms the presence of S_8 . The peaks around 166–170 eV in the samples indicate the presence of SO_4^{2-58} coming from the partial oxidation upon exposure to air during handling.

SEM images (Figure 7a–c') indicate that the resulting iodide intercalated LDH samples maintain the hexagonal prismatic shape of the LDH precursor, implying that the iodine adsorption process is followed by intercalation of the resulting I_3^- anions. EDS (Figure 8a' and Figure S3 and S4, Supporting Information) and elemental distribution maps (Figure 9 and Figure S3 and S4, Supporting Information) show the presence of a significant amount of S and I in the samples. Additionally,

iodine capture using K_2S_4 as a sorbent produces the KI cubic crystals, which was verified by the XRD pattern in Figure 1j. Clear evidence for the formation of KI was obtained from EDS and elemental distribution mapping (Figure 10).

Thermal Behavior of I-Laden Samples. The thermal decomposition behavior of the I-laden samples was studied with TG-DTA followed by EDS analysis of the residues. Figure 11 shows the TG-DTA curves of the I-laden samples along with the S_4 -LDH precursor for comparison. For S_4 -LDH-I, there were four obvious mass loss steps in the temperature ranges of 50–150, 150–250, 250–350, and 350–450 °C. The first step with the large mass loss of $\sim 40\%$ (50–150 °C) is attributed to the removal of physisorbed iodine and I_2 molecules from decomposition of I_3^- and perhaps some hydration water.⁶⁸ In addition, some sulfur loss could be occurring, which is consistent with the decrease of the S fraction as shown by EDS analyses, discussed below (Figure 8a',b'). The second and third mass loss steps (total $\sim 20\%$, 150–250 and 250–350 °C) appear to come from further removal of I_2 and S and dehydroxylation of brucite-like layers.^{68,72} The fourth step (350–500 °C) is attributed to the release of I^- due to subsequent sublimation of any metal iodide formed.

When the S_4 -LDH-I sample was heated in the air to 150, 350, and 450 °C for 1 h, the EDS analyses (see Figure 8) along with the elemental distribution maps showed a decrease of the S and I contents. The significant amount of iodine remaining in the 350 °C-heated sample corresponds to an I^- intercalated phase after the I_2 molecules were removed. The iodine content of the 450 °C-heated sample (Figure 8d') is drastically reduced ($\leq 1\%$ in atomic ratio), as the structure collapses, hydroxyl condensation to water occurs and the as-formed metal iodides evaporate. The elemental distribution maps of the residue (Figure 9d-4) confirmed the extremely low iodine content at this stage.

The variable temperature XRD (Figure 6) of I-laden samples (i.e., S_4 -LDH-I) was used to investigate the structural changes with increasing temperature. At 100 °C, the (003) reflection (0.81–0.82 nm) was absent, and this stems from the fact that the (006) reflection gains intensity from the very heavy intercalated $[I_3]^-$ ions, which place large electron density on the (006) basal planes, as shown in Figure 1h. Between 100 and 400 °C, a series of basal (00l) Bragg reflections being characteristic of a layered LDH phase were clearly observed as considerable I_2 loss lowered the electron density on the (006) basal planes, ultimately allowing the (003) plane associated with the brucite layer to be shown. In addition, the peak with d -spacing of 0.15 nm corresponding to the (110) plane of the 2D LDH sheets was clearly discernible. The consistent basal spacing of 0.81 nm (100–400 °C) suggests that the iodine remains intercalated in LDH as I^- and $[I_3]^-$ ions define the same gallery height. When the sample was heated to 450 °C, however, the XRD patterns changed dramatically, signaling the collapse of the layered structure. The halo at 0.21 nm can be assigned to MgO (Figure 6d). The spinel phase which should occur during LDH calcinations⁷³ was not discernible here. Any metal iodide species is expected to be volatile and sublimates out of the samples in these temperatures. This suggests a large transformation of the structure takes place in this temperature range. The results agree well with the TGA results discussed above, which show a significant mass loss in the range of 400–450 °C.

CONCLUDING REMARKS

The polysulfide-containing S_x -LDH intercalates are strong iodine vapor capture agents despite their low surface areas. The LDH layers act as a supporting substrate and provide these polysulfide compounds with a protective yet accessible space for iodine vapor. The reducing property of the polysulfide species is the driving force for the chemisorption of iodine. The I_2 molecules are reduced to I_3^- ions while the polysulfide ions oxidize to form S_8 . Moreover, there is a physisorption component to the process contributing to the already high efficiency for $I_2(g)$ capture. The S_2 -LDH, S_4 -LDH, and S_6 -LDH materials showed iodine capture capacities of 1.32, 1.52, and 1.43 g/g, reaching a high adsorption rate of 152% by weight. These are comparable to or higher than previously reported materials such as the best MOF materials with their highest I_2 uptake of 125%. The results reported here demonstrate that high surface area materials are not always necessary for the effective capture of massive amounts of iodine. Compared with the Ag^+ -loaded zeolitic materials or the Pt^{2+} -containing aerogels, the lower cost of environmentally safe and abundant elements of S_x -LDH combined with their significant iodine adsorption capacity make them promising for highly efficient $I_2(g)$ capture. The latter is of importance to manage radioactive waste iodide relevant to the nuclear energy industry.

ASSOCIATED CONTENT

Supporting Information

UV/vis absorption spectra for I-laden sample (S_4 -LDH-I) dispersed in acetonitrile; BET surface areas of S_2 -LDH and S_4 -LDH; SEM images; EDS and elemental distribution maps for Mg, Al, S, and I of S_2 -LDH-I and S_6 -LDH-I. This materials are available free of charge via the Internet at <http://pubs.acs.org>.

AUTHOR INFORMATION

Corresponding Author

*Tel. +1-847-467-1541. Fax: +1-847-491-5937. E-mail: mkanatzidis@northwestern.edu.

Notes

The authors declare no competing financial interest.

ACKNOWLEDGMENTS

This work is supported by the National Science Foundations of China (NSFC; Nos. 21271028, 51272030, and 21271001) and the Department of Energy USA (NEUP program, Project 12-3438).

REFERENCES

- (1) Kintisch, E. *Science* **2005**, *310*, 1406.
- (2) Ewing, R. C.; von Hippel, F. N. *Science* **2009**, *325*, 151.
- (3) Kuepper, F. C.; Feiters, M. C.; Olofsson, B.; Kaiho, T.; Yanagida, S.; Zimmermann, M. B.; Carpenter, L. J.; Luther, G. W.; Lu, Z.; Jonsson, M. *Angew. Chem., Int. Ed.* **2011**, *50*, 11598.
- (4) Saiz-Lopez, A.; Plane, J. M. C.; Baker, A. R.; Carpenter, L. J.; von Glasow, R.; Martin, J. C. G.; McFiggans, G.; Saunders, R. W. *Chem. Rev.* **2012**, *112*, 1773.
- (5) Lee, W.; Ojovan, M.; Stennett, M.; Hyatt, N. *Adv. Appl. Ceram.* **2006**, *105*, 3.
- (6) Lu, J. Y. *Coord. Chem. Rev.* **2003**, *246*, 327.
- (7) Ten Hoeve, J. E.; Jacobson, M. Z. *Energy Environ. Sci.* **2012**, *5*, 8743.
- (8) Garino, T. J.; Nenoff, T. M.; Krumhansl, J. L.; Rademacher, D. X. *J. Am. Ceram. Soc.* **2011**, *94*, 2412.
- (9) Lee, J.; Cha, D.; Oh, Y.; Ko, K.; Song, J. *J. Hazard. Mater.* **2009**, *164*, 67.
- (10) Kaplan, D. I.; Serne, R. J.; Parker, K. E.; Kutnyakov, I. V. *Environ. Sci. Technol.* **2000**, *34*, 399.
- (11) Miller, A.; Wang, Y. *J. Environ. Radioact.* **2014**, *133*, 35.
- (12) Chapman, K. W.; Chupas, P. J.; Nenoff, T. M. *J. Am. Chem. Soc.* **2010**, *132*, 8897.
- (13) Riebe, B.; Dultz, S.; Bunnenberg, C. *Appl. Clay Sci.* **2005**, *28*, 9.
- (14) Zeng, M.-H.; Wang, Q.-X.; Tan, Y.-X.; Hu, S.; Zhao, H.-X.; Long, L.-S.; Kurmoo, M. *J. Am. Chem. Soc.* **2010**, *132*, 2561.
- (15) Sava, D. F.; Rodriguez, M. A.; Chapman, K. W.; Chupas, P. J.; Greathouse, J. A.; Crozier, P. S.; Nenoff, T. M. *J. Am. Chem. Soc.* **2011**, *133*, 12398.
- (16) Liu, Q.-K.; Ma, J.-P.; Dong, Y.-B. *Chem. Commun.* **2011**, *47*, 7185.
- (17) Shi, X.; Yang, J.; Salvador, J. R.; Chi, M. F.; Cho, J. Y.; Wang, H.; Bai, S. Q.; Yang, J. H.; Zhang, W. Q.; Chen, L. D. *J. Am. Chem. Soc.* **2011**, *133*, 7837.
- (18) Chapman, K. W.; Sava, D. F.; Halder, G. J.; Chupas, P. J.; Nenoff, T. M. *J. Am. Chem. Soc.* **2011**, *133*, 18583.
- (19) Yin, Z.; Wang, Q.-X.; Zeng, M.-H. *J. Am. Chem. Soc.* **2012**, *134*, 4857.
- (20) Falaise, C.; Volkringer, C.; Facqueur, J.; Bousquet, T.; Gasnot, L.; Loiseau, T. *Chem. Commun.* **2013**, *49*, 10320.
- (21) Bennett, T. D.; Saines, P. J.; Keen, D. A.; Tan, J.-C.; Cheetham, A. K. *Chem.—Eur. J.* **2013**, *19*, 7049.
- (22) Luo, Y. H.; Yu, X. Y.; Yang, J. J.; Zhang, H. *CrystEngComm* **2014**, *16*, 47.
- (23) Wang, X.-L.; Qin, C.; Lan, Y.-Q.; Shao, K.-Z.; Su, Z.-M.; Wang, E.-B. *Chem. Commun.* **2009**, 410.
- (24) Long, D. L.; Hill, R. J.; Blake, A. J.; Champness, N. R.; Hubberstey, P.; Proserpio, D. M.; Wilson, C.; Schroder, M. *Angew. Chem., Int. Ed.* **2004**, *43*, 1851.
- (25) Riley, B. J.; Chun, J.; Ryan, J. V.; Matyáš, J.; Li, X. S.; Matson, D. W.; Sundaram, S. K.; Strachan, D. M.; Vienna, J. D. *RSC Adv.* **2011**, *1*, 1704.
- (26) Sánchez-Polo, M.; Rivera-Utrilla, J.; Salhi, E.; Von Gunten, U. *J. Colloid Interface Sci.* **2006**, *300*, 437.
- (27) Katsoulidis, A. P.; He, J. Q.; Kanatzidis, M. G. *Chem. Mater.* **2012**, *24*, 1937.
- (28) Riley, B. J.; P, D. A.; Chun, J.; Matyáš, J.; Lepry, W. C.; Garn, T. G.; Law, J. D.; Kanatzidis, M. G. *Environ. Sci. Technol.* **2014**, *48*, 5832.
- (29) Riley, B. J.; Chun, J.; Um, W.; Lepry, W. C.; Matyas, J.; Olszta, M. J.; Li, X. H.; Polychronopoulou, K.; Kanatzidis, M. G. *Environ. Sci. Technol.* **2013**, *47*, 7540.
- (30) Mohanan, J. L.; Arachchige, I. U.; Brock, S. L. *Science* **2005**, *307*, 397.
- (31) (a) Bag, S.; Trikalitis, P. N.; Chupas, P. J.; Armatas, G. S.; Kanatzidis, M. G. *Science* **2007**, *317*, 490. Shafaei-Fallah, M.; He, J. Q.; Rothenberger, A.; Kanatzidis, J. *J. Am. Chem. Soc.* **2011**, *133*, 1200–1202.
- (32) Oh, Y.; Morris, C. D.; Kanatzidis, M. G. *J. Am. Chem. Soc.* **2012**, *134*, 14604.
- (33) Khan, A. I.; O'Hare, D. *J. Mater. Chem.* **2002**, *12*, 3191.
- (34) Constantino, V. R.; Pinnavaia, T. J. *Catal. Lett.* **1994**, *23*, 361.
- (35) Corma, A.; Fornes, V.; Rey, F.; Cervilla, A.; Llopis, E.; Ribera, A. *J. Catal.* **1995**, *152*, 237.
- (36) Costantino, U.; Costantino, F.; Elisei, F.; Latterini, L.; Nocchetti, M. *Phys. Chem. Chem. Phys.* **2013**, *15*, 13254.
- (37) Gérardin, C.; Kostadinova, D.; Sanson, N.; Coq, B.; Tichit, D. *Chem. Mater.* **2005**, *17*, 6473.
- (38) Rives, V.; Angeles Ulibarri, M. *Coord. Chem. Rev.* **1999**, *181*, 61.
- (39) Fogg, A. M.; Williams, G. R.; Chester, R.; O'Hare, D. *J. Mater. Chem.* **2004**, *14*, 2369.
- (40) Yan, D. P.; Lu, J.; Ma, J.; Qin, S. H.; Wei, M.; Evans, D. G.; Duan, X. *Angew. Chem., Int. Ed.* **2011**, *50*, 7037.
- (41) Vialat, P.; Mousty, C.; Taviot-Gueho, C.; Renaudin, G.; Martinez, H.; Dupin, J. C.; Elkaim, E.; Leroux, F. *Adv. Funct. Mater.* **2014**, *24*, 4831.

- (42) Zhao, Y.; He, S.; Wei, M.; Evans, D. G.; Duan, X. *Chem. Commun.* **2010**, 46, 3031.
- (43) Ma, S. L.; Fan, C. H.; Du, L.; Huang, G. L.; Yang, X. J.; Tang, W. P.; Makita, Y.; Ooi, K. *Chem. Mater.* **2009**, 21, 3602.
- (44) Xue, X. Y.; Gu, Q. Y.; Pan, G. H.; Liang, J.; Huang, G. L.; Sun, G. B.; Ma, S. L.; Yang, X. J. *Inorg. Chem.* **2014**, 53, 1521.
- (45) Mohanambe, L.; Vasudevan, S. *Inorg. Chem.* **2004**, 43, 6421.
- (46) Ma, S. L.; Chen, Q. M.; Li, H.; Wang, P. L.; Islam, S. M.; Gu, Q. Y.; Yang, X. J.; Kanatzidis, M. G. *J. Mater. Chem. A* **2014**, 2, 10280.
- (47) Ma, S. L.; Shim, Y.; Islam, S. M.; Subrahmanyam, K. S.; Wang, P. L.; Li, H.; Wang, S. C.; Yang, X. J.; Kanatzidis, M. G. *Chem. Mater.* **2014**, 26, 5004.
- (48) Iyi, N.; Matsumoto, T.; Kaneko, Y.; Kitamura, K. *Chem. Mater.* **2004**, 16, 2926.
- (49) Ma, S. L.; Du, L.; Wang, J.; Chu, N. K. i.; Sun, Y. H.; Sun, G. B.; Yang, X. J.; Ooi, K. *Dalton Trans.* **2011**, 40, 9835.
- (50) Ma, S. L.; Wang, J.; Du, L.; Sun, Y. H.; Gu, Q. Y.; Sun, G. B.; Yang, X. J. *J. Colloid Interface Sci.* **2013**, 393, 29.
- (51) Miyata, S. *Clays Clay Miner.* **1975**, 23, 369.
- (52) Yamaoka, T.; Abe, M.; Tsuji, M. *Mater. Res. Bull.* **1989**, 24, 1183.
- (53) Nakato, T.; Kuroda, K.; Kato, C. *Chem. Mater.* **1992**, 4, 128.
- (54) Vermeulen, L. A.; Thompson, M. E. *Nature* **1992**, 358, 656.
- (55) Janz, G.; Coutts, J.; Downey, J., Jr; Roduner, E. *Inorg. Chem.* **1976**, 15, 1755.
- (56) Islam, S. M.; Im, J.; Freeman, A. J.; Kanatzidis, M. G. *Inorg. Chem.* **2014**, 53, 4698.
- (57) Smart, R. S. C.; Skinner, W. M.; Gerson, A. R. *Surf. Interface Anal.* **1999**, 28, 101.
- (58) Moulder, J. F.; Stickle, W. F.; Sohol, P. E.; Bomben, K. D. *Handbook of X-ray Photoelectron Spectroscopy*; Chastain, J., King, R. C., Jr. Ed.; Physical Electronics, Inc.: Eden Prairie, 1995.
- (59) Klopogge, J. T.; Wharton, D.; Hickey, L.; Frost, R. L. *Am. Mineral.* **2002**, 87, 623.
- (60) Al-Attar, L.; Dyer, A. J. *Mater. Chem.* **2002**, 12, 1381.
- (61) Klabo, P. J. *Am. Chem. Soc.* **1967**, 89, 3667.
- (62) Svensson, P. H.; Kloo, L. *Chem. Rev.* **2003**, 103, 1649.
- (63) Nour, E.; Chen, L.; Laane, J. J. *Phys. Chem.* **1986**, 90, 2841.
- (64) Xin, B.; Zeng, G.; Gao, L.; Li, Y.; Xing, S.; Hua, J.; Li, G.; Shi, Z.; Feng, S. *Dalton Trans.* **2013**, 42, 7562.
- (65) Gabes, W.; Stufkens, D. J. *Spectrochim. Acta A* **1974**, A 30, 1835.
- (66) Gabes, W.; Stufkens, D. J.; Gerding, H. J. *Mol. Struct.* **1973**, 17, 329.
- (67) Ma, R.; Liang, J.; Takada, K.; Sasaki, T. *J. Am. Chem. Soc.* **2011**, 133, 613.
- (68) Bastianini, M.; Costenaro, D.; Bisio, C.; Marchese, L.; Costantino, U.; Vivani, R.; Nocchetti, M. *Inorg. Chem.* **2012**, 51, 2560.
- (69) Sava, D. F.; Rodriguez, M. A.; Chapman, K. W.; Chupas, P. J.; Greathouse, J. A.; Crozier, P. S.; Nenoff, T. M. *J. Am. Chem. Soc.* **2011**, 133, 12398.
- (70) Kentjono, L.; Liu, J.; Chang, W.; Irawan, C. *Desalination* **2010**, 262, 280.
- (71) Prasanna, S. V.; Kamath, P. V.; Shivakumara, C. *J. Colloid Interface Sci.* **2010**, 344, 508.
- (72) Zhao, H.; Vance, G. F. *J. Am. Chem. Soc.* **1997**, 1961.
- (73) Rives, V. *Inorg. Chem.* **1999**, 38, 406.
- (74) Park, K. S.; Ni, Z.; Cote, A. P.; Choi, J. Y.; Huang, R. D.; Uribe-Romo, F. J.; Chae, H. K.; O'Keeffe, M.; Yaghi, O. M. *Proc. Natl. Acad. Sci. U. S. A.* **2006**, 103, 10186.
- (75) Solis-Ibarra, D.; Hemamala, I. K. *Angew. Chem., Int. Ed.* **2014**, 53, 1039.